Numerical modelling of dynamic pressure and flow in hopper discharge using the Arbitrary Lagrangian–Eulerian formulation

Engineering Structures 56 (2013) 1308–1320

Contents lists available at ScienceDirect

Engineering Structures

journal homepage: www.elsevier.com/locate/engstruct

Numerical modelling of dynamic pressure and flow in hopper discharge using the Arbitrary Lagrangian–Eulerian formulation

Yin Wang [a,b,*], Yong Lu [b], Jin Y. Ooi [b]

[a] Institute of Geotechnical Engineering, School of Civil Engineering, Dalian University of Technology, Dalian, 116024, China
[b] Institute for Infrastructure and Environment, School of Engineering, University of Edinburgh, UK

ARTICLE INFO

Article history:
Received 1 May 2012
Revised 25 March 2013
Accepted 3 July 2013
Available online 7 August 2013

Keywords:
Conical hopper
Silo discharge's finite element (FE) analysis
Arbitrary Lagrangian–Eulerian formulation (ALE)
Dynamic pressure
Granular flow

ABSTRACT

Silos and hoppers are commonly used for the storage and handling of bulk solids in industry. Although the pressures acting on the silo walls during filling are well understood, an accurate prediction of pressures during discharge remains an important open problem for silo design. This paper describes a finite element analysis of the granular flow in a conical hopper to investigate the dynamic pressure and flow during discharge. The behaviour of the stored solid is modelled using a continuum mechanics approach formulated in an Arbitrary Lagrangian–Eulerian (ALE) frame of reference. With the aid of the ALE approach, in principle almost a complete silo discharge process may be simulated satisfactorily without mesh distortion problems, which are often encountered in modelling silo discharge using a continuum approach. Temporally averaged discharge pressure distribution is evaluated from the FE simulation and found to be in good agreement with the commonly quoted theoretical solution. Significant pressure fluctuations are predicted during the initial discharge period, which are comparable to the fluctuating pressure patterns reported in some silo discharge experiments. Spectral analysis of the predicted pressure fluctuation reveals two dominant frequencies. The causes for these frequency events have been investigated thoroughly in the paper, which lead to the conclusion that compression wave propagation and intermittent shear zones within the granular solid are responsible for the higher and lower frequency event respectively. These dynamic events provide a plausible explanation for silo quaking and vibration that are associated with silo discharge. Further parametric study has also been performed to investigate the effect of discharge velocity and wall roughness on these dynamic events.

1. Introduction

Silos and hoppers are widely used for the storage and handling of bulk solids in industry. In the design of silos, the pressure acting on the silo walls during filling and discharge are the main loads that need to be determined for design. Silo pressures during filling and storing are generally accepted to be well represented by Janssen type pressure equation [1]. However during discharge, the silo pressure tends to exhibit time and space variations and more work is required to determine the discharge pressure more accurately. With the general lack of understanding and information with regard to discharge process, most national standards have defined discharge pressure for silos simply using a multiplication factor applied to the filling pressure based on Janssen's theory and its improvement in different ways by other authors [2]. More recently Eurocode has introduced additional patch loads to account for the accidental asymmetries of loading associated with eccentricities in the filling and discharge process [2]. It is evident from silo experiments [3–7] that silo pressure during discharge can be quite different from that during filling.

Whilst finite element (FE) predictions [8–10] of wall pressure at the end of filling stage are in good agreement with both theoretical solutions and experimental observations, the FE modelling of the wall pressures during discharge is relatively rare and requires more fundamental research. Rombach and Eibl [11] performed a dynamic FE analysis and presented dynamic pressure profiles dependent on space and time just at the beginning of emptying stage. In other studies, either remesh–rezoning technique or assumed failure boundary was used to describe large deformation occurring during the discharge stage in order to avoid mesh distortions [12,13].

This paper presents a FE simulation of a conical hopper discharge to investigate the dynamic characteristics of the pressure and flow during discharge. The FE simulation is performed using the uncoupled Arbitrary Lagrangian–Eulerian (ALE) formulation with an adaptive meshing technique using the commercial FE software Abaqus [14]. This method allows for the simulation of almost the entire silo discharge process without involving the mesh distortion problem which is often encountered in the modelling of granular flow [12,15]. To simplify the simulation whilst an

* Corresponding author. Tel.: +44 0 7889215716.
E-mail addresses: wangyin47@gmail.com, yin.wang@ed.ac.uk (Y. Wang).

0141-0296/$ - see front matter © 2013 Elsevier Ltd. All rights reserved.
http://dx.doi.org/10.1016/j.engstruct.2013.07.006

emphasis is placed on the primary dynamic phenomena, an axisymmetric approach [16] is adopted with a simple wall boundary condition, whereas a simple constitutive model is adopted for bulk solids.

Using the above ALE-based approach, the primary dynamic events during silo discharge can be simulated explicitly. The responses predicted from the simulation are studied to provide further insight into the fluctuating pressure patterns observed in silo discharge experiments. Temporally averaged discharge pressure distribution is evaluated and used to compare with theoretical solutions. Power spectral analysis of the predicted pressure fluctuation reveals two dominant frequencies, and the cause for these frequency events are investigated thoroughly. Further parametric study with the FE model is also performed to investigate the effect of discharge velocity and wall roughness on the wall pressure fluctuations.

2. Background theories

2.1. Classical hopper pressure theories

The determination of pressure acting on the silo wall is a classic topic that has been studied ever since Janssen [1] first proposed an analytical solution of the differential equation corresponding to the vertical equilibrium of a horizontal slice of solid in a cylindrical silo. The Janssen equation has been adopted as a theoretical basis in most national standards. Walker [17] improved Janssen's analysis to determine silo pressure in the cylindrical part by considering in greater detail the actual stress distribution in the wall region, and extended it to the case of conical hoppers. Using the slice element method, Walker gave the solution to the pressure acting on the hopper wall as:

$$p_{nw} = (\sigma_{hh})_w \frac{1+\sin\phi\cos(\omega+\phi_w)}{1-\sin\phi\cos(\omega+\phi_w+2\alpha)} \tag{1}$$

in which

$$(\sigma_{hh})_w = \frac{\gamma h'}{m-1}\left[1-\left(\frac{h'}{h_a}\right)^{m-1}\right] + Q_0\left(\frac{h'}{h_a}\right)^m \tag{2}$$

$$\sin\omega = \frac{\sin\phi_w}{\sin\phi} \tag{3}$$

$$m = \frac{2\sin\phi\sin(\omega+\kappa\phi_w+2\kappa\alpha)}{\tan\alpha\{1-\kappa\sin\phi\cos(\omega+\kappa\phi_w+2\kappa\alpha)\}} \tag{4}$$

where α is the hopper apex half angle; $(\sigma_{hh})_w$ denotes the horizontal stress acting at the wall; q_0 is the uniform surcharge acting on the top surface of the stored solid in the hopper; in the case under consideration here, there is no applied stress on the top surface and so $q_0 = 0$; p_{nw} is the wall normal pressure; h' is the height of material measured vertically from the apex of hopper; h_a is the hopper height measured from the apex; ϕ is the effective angle of internal friction of the stored solid; ϕ_w is the hopper wall friction angle and γ is the specific weight of the stored solid; κ is a constant with $\kappa = -1$ for filling and storing, and $\kappa = 1$ for discharge [18].

As far as discharge is concerned, Eurocode [19] evaluates the discharge pressure by applying equations based on the Walker's theory. The Walker's method is deemed to be appropriate to compare with the present FE simulation for the conical hopper discharge.

2.2. Empirical equation of flow rate

There exist a number of prediction methods for the mass flow rate in silo discharge. In general, the mass flow rate depends on material bulk density ρ_b, particle size of material d, acceleration due to gravity g, orifice diameter of the container D_0, and the coefficient of wall friction μ_w. Thus,

$$W_B = f(\rho_b, g, D_0, \mu_w, d) \tag{5}$$

Beverloo et al. [20] proposed the following prediction formula:

$$W_B = C\rho_b\sqrt{g}(D_0-\lambda d)^{5/2} \tag{6}$$

where C is deemed to be slightly dependent on μ_w and normally takes a value close to 0.58. A large value as 0.64 should be given to exceptionally smooth particles such as spherical glass beads. The coefficient λ is about 1.5 for spherical particles but takes somewhat larger values for angular particles [18].

It should be noted that Beverloo equation is applicable only for cylindrical bunkers and funnel flow hoppers. In mass flow conical hopper, the effect of the apex half-angle α becomes important. Nedderman [18] extended Beverloo's formula by incorporating the statement given by Rose and Tanaka [21] for mass flow conical hopper:

$$W = W_B F(\alpha, \phi_d) \tag{7}$$

where W_B is the mass flow rate predicted from the Beverloo's formula as given in Eq. (6) and $F(\alpha, \phi_d)$ is given by

$$\begin{aligned} &F(\alpha,\phi_d) = (\tan\alpha\tan\phi_d)^{-0.35} \quad \text{for } \alpha < 90^0 - \phi_d \\ &F = 1 \quad \text{for } \alpha > 90^0 - \phi_d \end{aligned} \tag{8}$$

in which ϕ_d is the angle between the stagnant zone boundary and the horizontal.

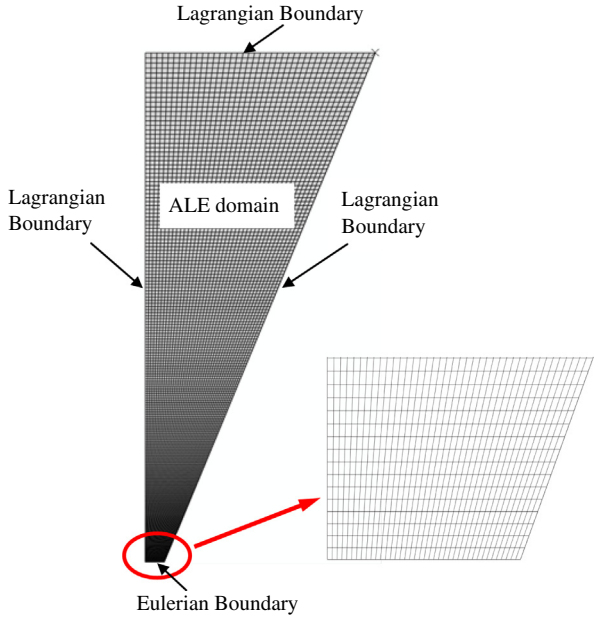

Fig. 1. Discretization grid and ALE boundaries.

Table 1
Material parameters.

Bulk density (ρ_b)	1000 kg/m^3
Young's modulus (E)	5.5 e5 Pa
Poisson's ratio (v)	0.3
Internal angle of friction (ϕ_i)	30°
Dilation angle (ψ)	10°
Coefficient of solid-wall friction ($\tan\phi_w$)	0.267

3. FE model and ALE implementation

To avoid mesh distortion due to large material deformation, the entire hopper discharge process is simulated using the so-called uncoupled Arbitrary Lagrangian–Eulerian (ALE) formulation in the Abaqus/Explicit program [14]. The ALE approach is a particular extension of the Lagrangian formulation [22]. In this approach, the mesh motion is taken arbitrarily from material deformation to keep element shape optimal, especially under large material deformation. A Lagrangian phase is first carried out which obtains the required convergence; secondly, an Eulerian phase combined with

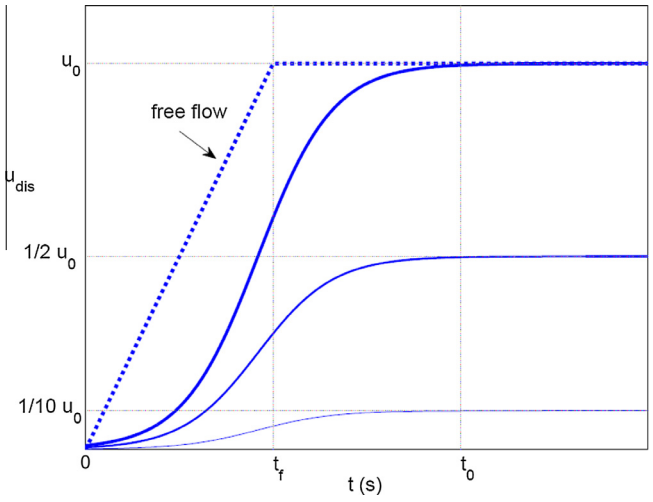

Fig. 2. Time series of central node velocity in the free flow and several controlled flow scenarios.

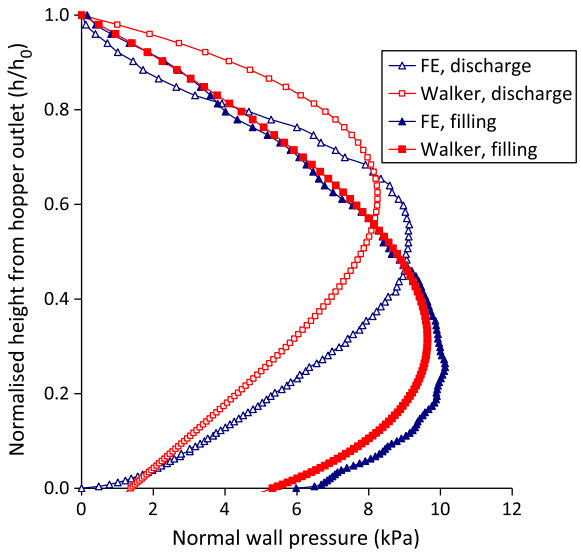

Fig. 3. Comparison between numerical and theoretical predictions of wall normal pressure distributions along the hopper wall for end of filling and beginning of discharge (discharge pressure averaged over first 10 s of discharge).

Table 2
Parameters used in the extended Beverloo equation [18].

C	D_0 (m)	λ	d	α (°)	ϕ_d (°)	ρ_b (kg/m^3)
0.58	0.2	1.5	0	22	45	1000

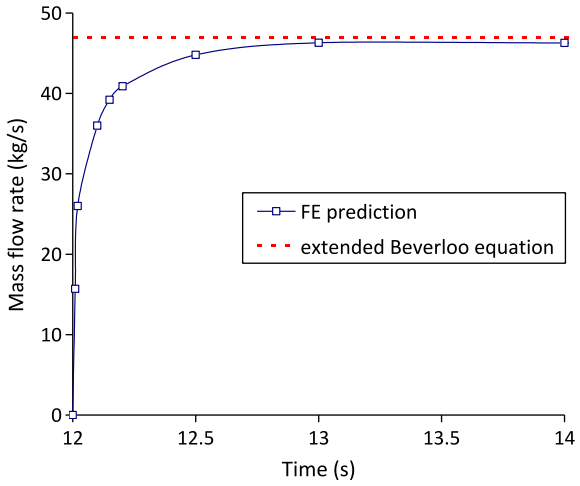

Fig. 4. Comparison of FE calculated mass flow rate with extended Beverloo equation [18] for flow under gravity.

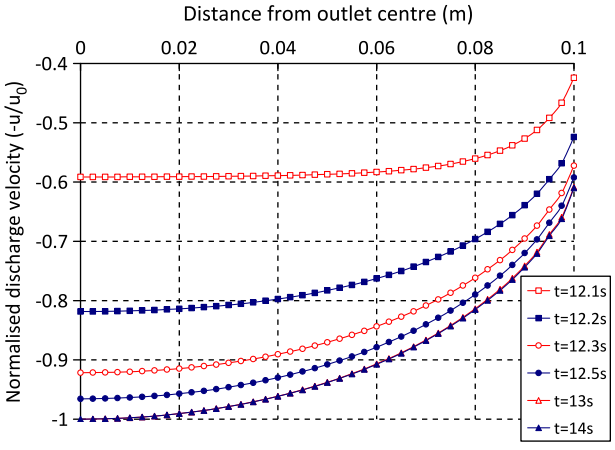

Fig. 5. Discharge velocity profiles along the hopper outlet at various time points.

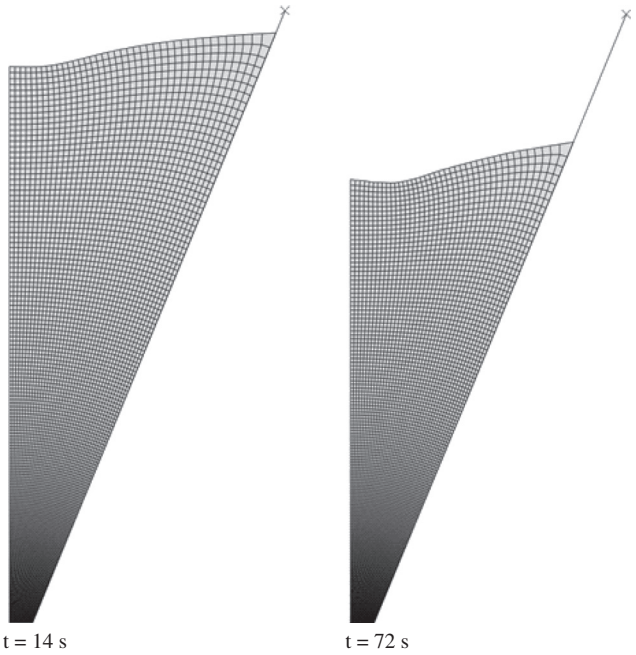

Fig. 6. Deformed mesh of granular solid at two different discharge time points.

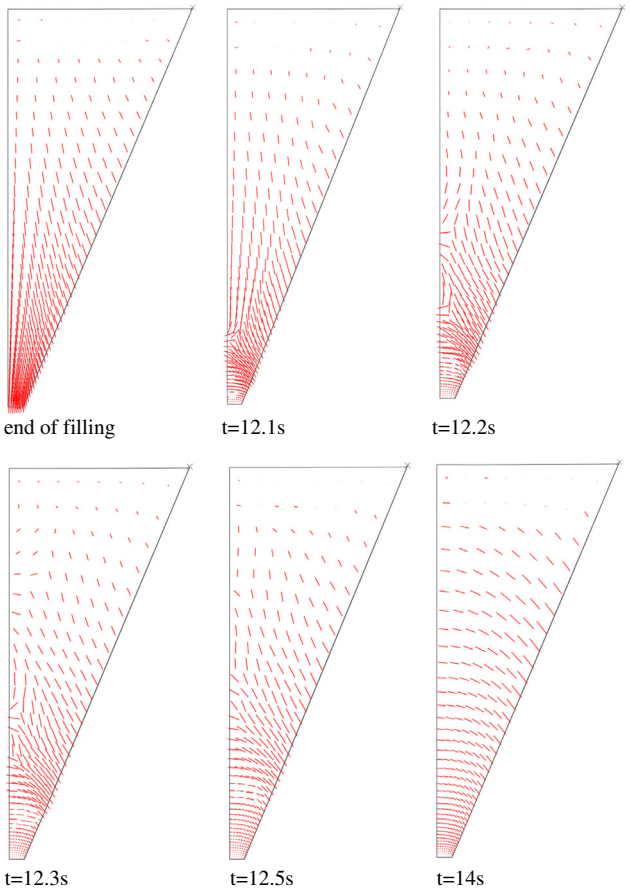

Fig. 7. Major principal stress orientation at various discharge time points.

a smoothing phase is performed. In the smoothing phase, the mesh configuration is adjusted by moving element nodes in an appropriate way so as to control mesh distortion. By doing so, the mesh topology remains similar and the number of nodes and elements are kept constant. In turn, in the Eulerian phase, a remap of the solution of the Lagrangian phase onto the new mesh is performed by taking into account all convective effects. A more detailed description of the ALE technique can be found in Ref. [23].

3.1. Hopper model geometry and material properties

A conical hopper with an axisymmetrical geometry is considered in the present FE simulation. The height h_0 of the hopper is 2.64 m, radius at the top 1.2 m, radius at the bottom 0.1 m and apex half-angle $\alpha = 22°$.

In the FE simulation, the stored granular solid is modelled as an elastic-perfectly plastic material using a Drucker–Prager failure criterion [24]. Following a mesh convergence study, a fine mesh of 8000 first-order 4-node quadrilateral elements with reduced integrations is used to model the granular solid (see Fig. 1), which is found to be sufficient to ensure a satisfactory convergence of the stress computations. The walls are modelled using 2-node rigid elements, and their interactions with granular solids are modelled using Coulomb type contact with a constant coefficient of wall friction.

The material properties are chosen to represent a fictitious material that is commonly used in FE modelling of silo discharge by other authors [12,25–27]. The assumed material parameters are presented in Table 1.

An explicit time integration scheme is employed to perform the non-linear dynamic analysis. A convergence study concerning the time increment has been performed and a time increment of the order of 1×10^{-6} s is required so as to ensure a stable solution. Geometric non-linearity is taken into account. To limit numerical oscillations, the default linear and quadratic viscosity pressure in Abaqus is used [14] which is not included in the material point stress. In the ALE, both Lagrangian and Eulerian boundaries are used. The sides and top surface of the material are defined as Lagrangian boundaries while the base (outlet) is set to be an Eulerian boundary as shown in Fig. 1. An Eulerian boundary can never overlap a Lagrangian boundary and by default, the corner points at the hopper outlet are subject to the Lagrangian boundary condition in Abaqus. This configuration permits the stored solid to deform and flow within the hopper whilst eliminating the potential mesh distortion problem at the outlet. A fuller description of the ALE boundary definition can be found in Ref. [14].

3.2. Modelling the filling and discharging states

The whole numerical process contains two main stages of analyses: the first is for filling and the second is for discharge. The filling state in the hopper is modelled by discretizing the final

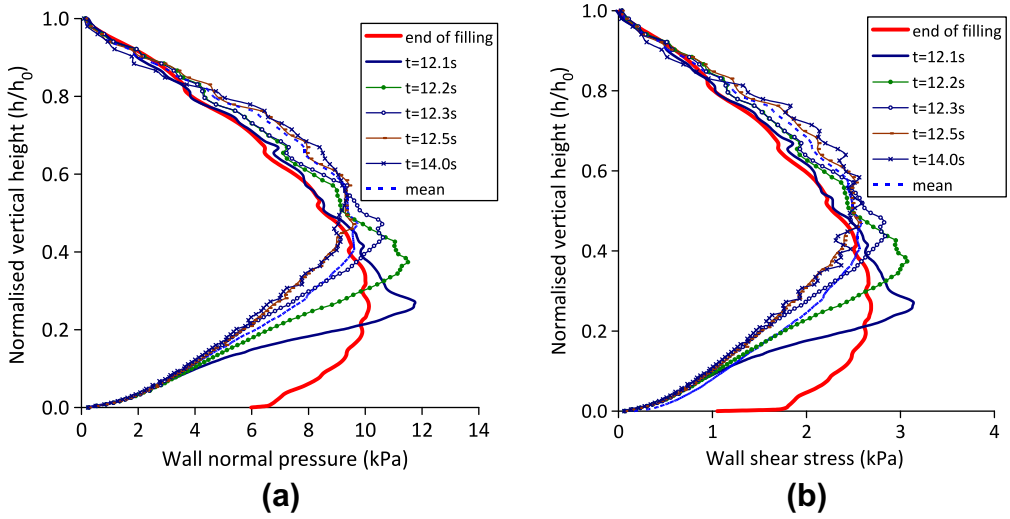

Fig. 8. Wall pressure distributions at various time points (mean value obtained by averaging from 12.1 s to 14.0 s): (a) wall normal pressure; (b) wall shear stress.

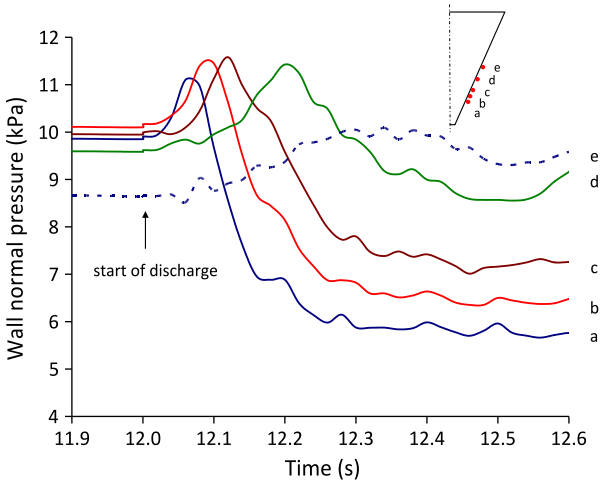

Fig. 9. Time series of normal wall pressure at several points on hopper walls during initial discharge.

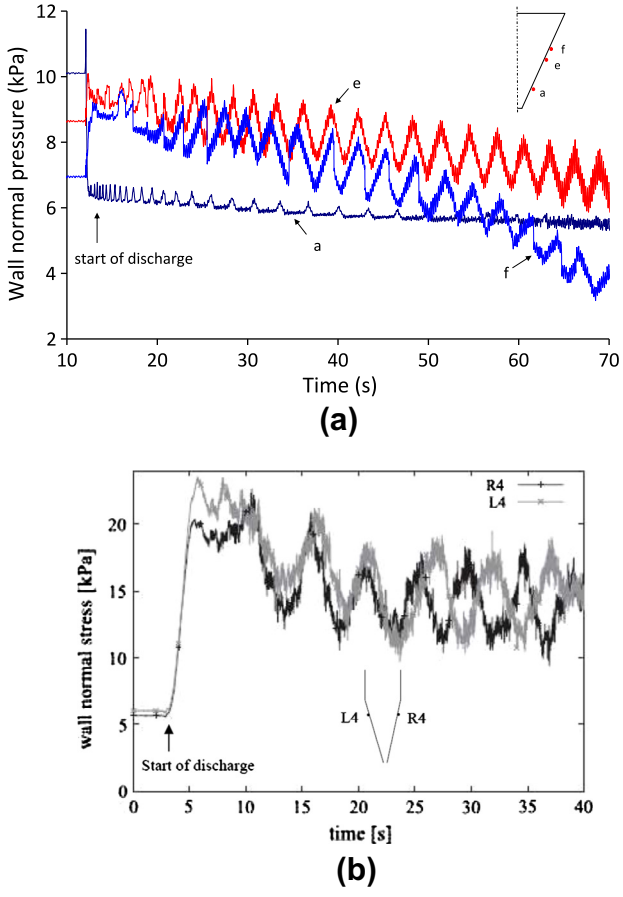

Fig. 10. Time series of normal wall pressure at different points on hopper walls during discharge: (a) FE simulation for flow under gravity; (b) experimental measurement for controlled flow at a relatively slow speed (after Ostendorf et al.) [31].

geometry of the solid fill into ten layers and then activating each layer sequentially in the FE analysis starting from the bottom layer. The numerical process involved achieving equilibrium for each activated layer under the load of gravity before the next layer is laid on with a "stress free" state, thereby simulating the progressive filling process [28]. To avoid numerical oscillation

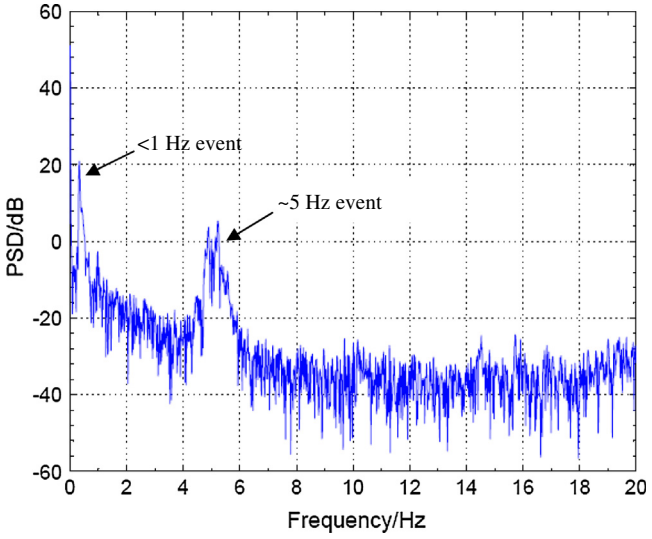

Fig. 11. Power spectral density estimation of the numerically calculated wall pressure at point *e* for the whole process of discharge (t = 12–72 s).

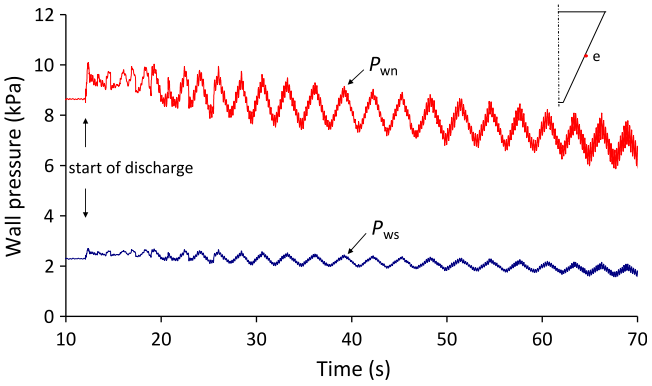

Fig. 12. Time series of wall normal pressure and shear stress at wall point *e*.

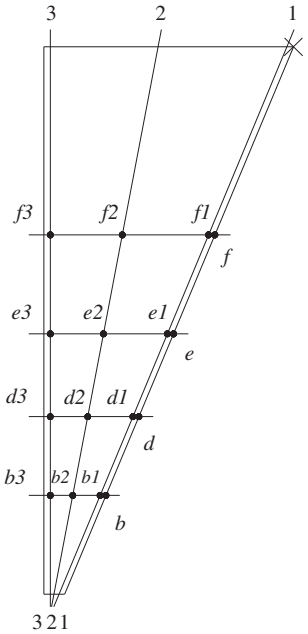

Fig. 13. Locations of representative points and sections.

due to sudden loading, the load of gravity is applied in a smooth manner by using the 3rd order built-in load amplitude function in Abaqus [14]. The top surface of the solid is at the top of the hopper.

To simulate the discharge process, a gravitational free flow is first considered by removing the constraints at the hopper outlet instantaneously. The numerical outcome displayed in Fig. 2 shows that the discharge velocity at the central node of the outlet increases rapidly and then reaches a constant level u_0 at $t = t_f$. For

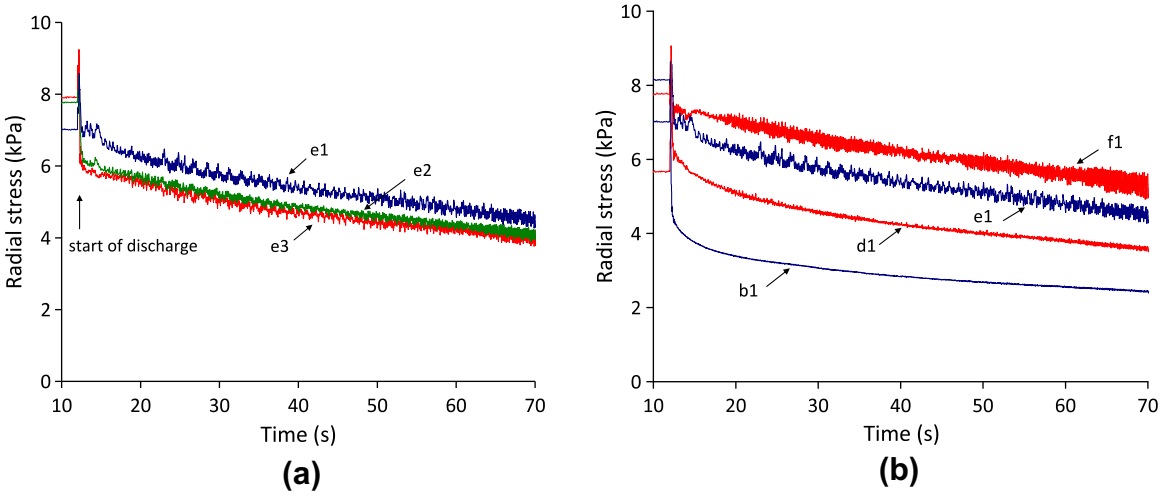

Fig. 14. Time series of radial stress at different points: (a) along a horizontal direction; (b) along a generator direction (section 1-1).

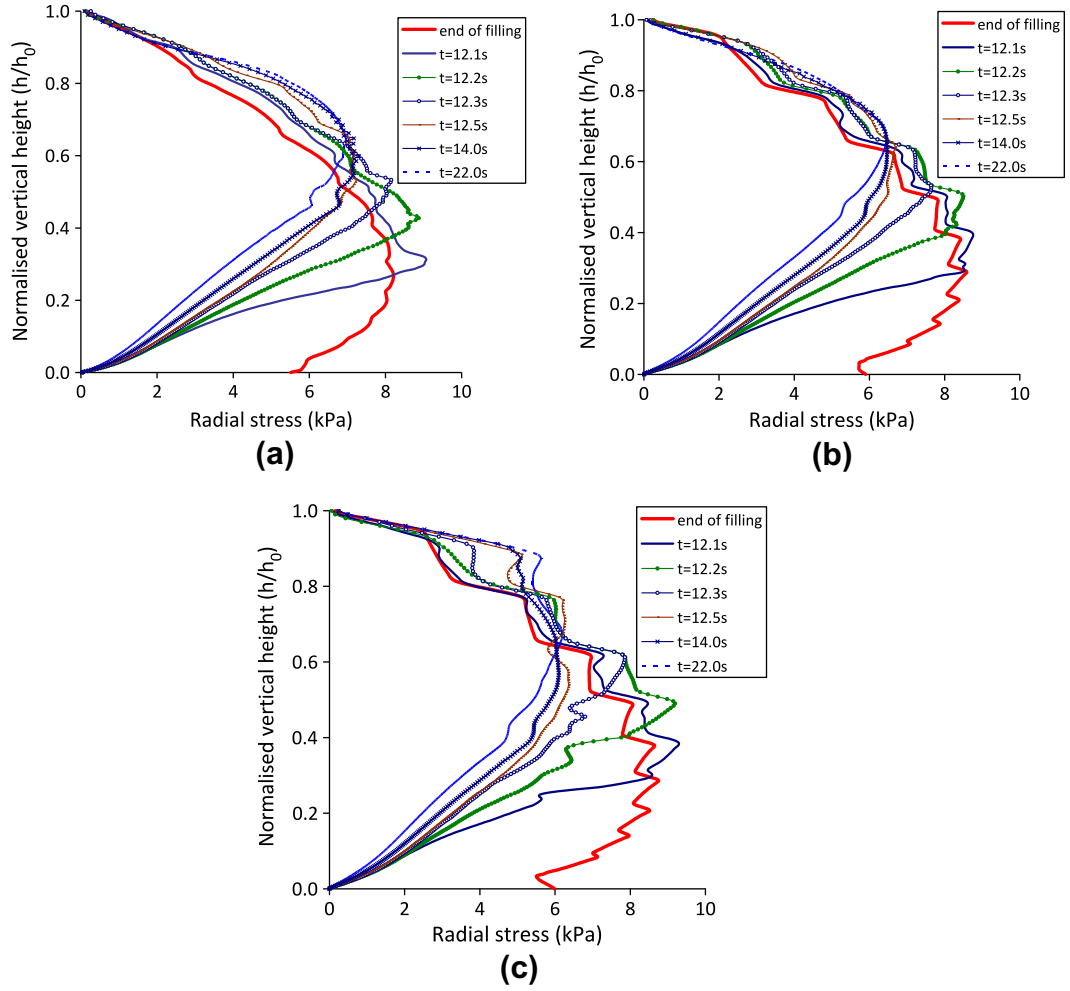

Fig. 15. Distributions of radial stresses at three generator sections at various time points: (a) section 1-1; (b) section 2-2; and (c) section 3-3.

the purpose of comparison, discharge under a controlled flow is also simulated. This is numerically achieved by accelerating the boundary downwards until it reaches a specified velocity which is then kept constant after $t = t_0$ where t_0 is usually set to be longer than t_f for the free flow, herein $t_0 = 2t_f$. A series of constant velocities ($u_{dis} = u_0$, $0.5u_0$, $0.1u_0$) for the controlled flow have been considered in the present FE simulations, as shown in Fig. 2.

4. General FE results and comparison with theories

To verify the present numerical model and demonstrate its ability for hopper discharge simulation, we consider comparisons with Walker's solution for hopper wall pressure and extended Beverloo equation for mass flow rate.

4.1. Comparison with hopper pressure theory

The calculated normal pressure distributions along the hopper wall during filling and discharge are compared with the theoretical solution, namely Walker's method [17] in Fig. 3. Since a truncated conical hopper is used in the numerical model (as would be the case in a real hopper), the theoretical solutions are computed to the truncated height. The wall pressures calculated by the present FE simulation are temporally averaged over the first 10 s period after the start of discharge. Doing so has two purposes: one is to smooth out the transient effects on wall pressures at the beginning of discharge (the transient effects are studied separately later); and the other is to ensure that the hopper is effectively still fully filled with granular solid in a short period of discharge. The pressure at representative locations on the wall is extracted at every time point over an interval of 10 s with a sampling rate of 50 Hz. The averaged pressure is determined by a simple arithmetic mean via the following equation:

$$p_{wn} = \frac{1}{N}\sum_{i=1}^{N} p_{wn(i)} \tag{9}$$

where $p_{wn(i)}$ represents the normal pressure at a specified wall point at the ith time point and p_{wn} is the average normal pressure at the corresponding wall point from the N time points over the specified interval.

From Fig. 3, a good agreement can be seen between the numerical and theoretical prediction of wall pressure at the end of the filling process. For the discharge pressure, it is clearly seen that the numerically calculated pressure pattern also follows the theoretical solution well. Namely, the pressure peaks move from the lower part to the higher part of the hopper. Some difference in discharge pressure distributions between the numerical and theoretical prediction is not surprising since Walker's solution for the discharge state is complying with the static equilibrium in the conical hopper, whilst the numerical simulation is considering not only the static equilibrium but the varying filling level of the stored solid.

4.2. Comparison with empirical equation of flow rate

A comparison of mass flow rate prediction between the numerical result and the extended Beverloo equation [18] has been performed to further verify the present FE model. The relevant parameters for the extended Beverloo equation are chosen according to published experimental results [18] and summarised in Table 2. In the absence of more reliable information, the recommendation from Nedderman [18] of $\phi_d = 45°$ is assumed and d is set to be zero because the stored solid particle of very small radius is considered. The mass flow rate from the FE simulation is evaluated from the product of the solid density, the area of the hopper outlet and the discharge velocity profile at the outlet. Whilst the extended Beverloo equation gives a constant mass flow rate, a progressively increase flow rate is predicted by the present FE simulation until a steady discharge velocity is achieved about 2 s after discharge starts. From Fig. 4, it is clearly seen that the fully developed flow rate from the FE simulation matches the extended Beverloo empirical equation very well.

5. Dynamic effects during discharge

5.1. Transient phenomena during initial discharge

The present FE analysis simulates a total time of 72 s. The period for filling is from $t = 0$–10 s, and a storage period of 2 s is set prior to the start of the discharge process. The discharge process is simulated from $t = 12$–72 s with a duration of 60 s.

The evolution of velocity profile at the beginning of discharge for the free flow case is shown in Fig. 5. A parabolic profile develops with the maximum velocity at the centre of the outlet. The discharge velocity profile reaches its asymptotic state at $t = 14$ s, about 2 s after the start of discharge (with $u_0 \approx 1.0$ m/s). The deformed geometries of the granular solid at an early stage of discharge and at a late stage are shown in Fig. 6.

The stress field within the granular solid experiences a switch from a predominantly active (the major principal stresses are largely vertically oriented) to a passive state (the major principal

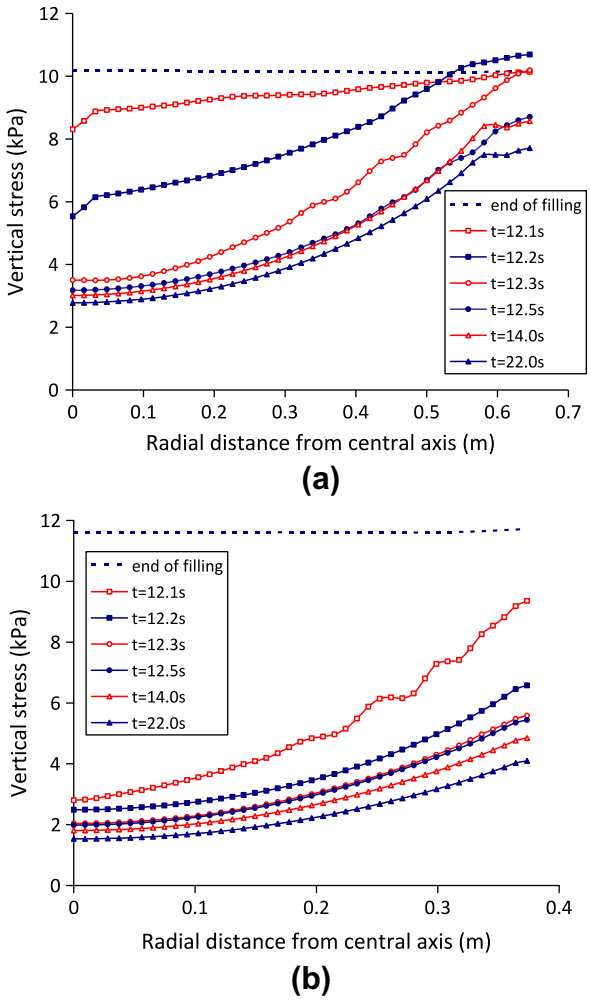

Fig. 16. Distribution of vertical stress at various time points: (a) along section *e*-*e*; (b) along section *b*-*b*.

stresses are horizontally oriented) [18]. Herein the major principal stress orientations computed at the selected six time instances during incipient discharge are shown in Fig. 7. The switch of the stress state propagates from the bottom to the top of the hopper and brings passive stress state to the whole flowing zone. As such, an "arched" stress field is formed in much of the hopper, and this is consistent with existing observations [29]. A similar switch of stress field, which is used to identify the flow pattern (either mass or funnel flow), has been reported in the FE modelling of silo discharge [30].

Fig. 8 shows the evolution of the normal pressure and shear stress at the hopper walls during the initial period of discharge. The mean values are obtained by temporally averaging over the first 2 s after discharge started at t = 12.0 s. From this figure, it is

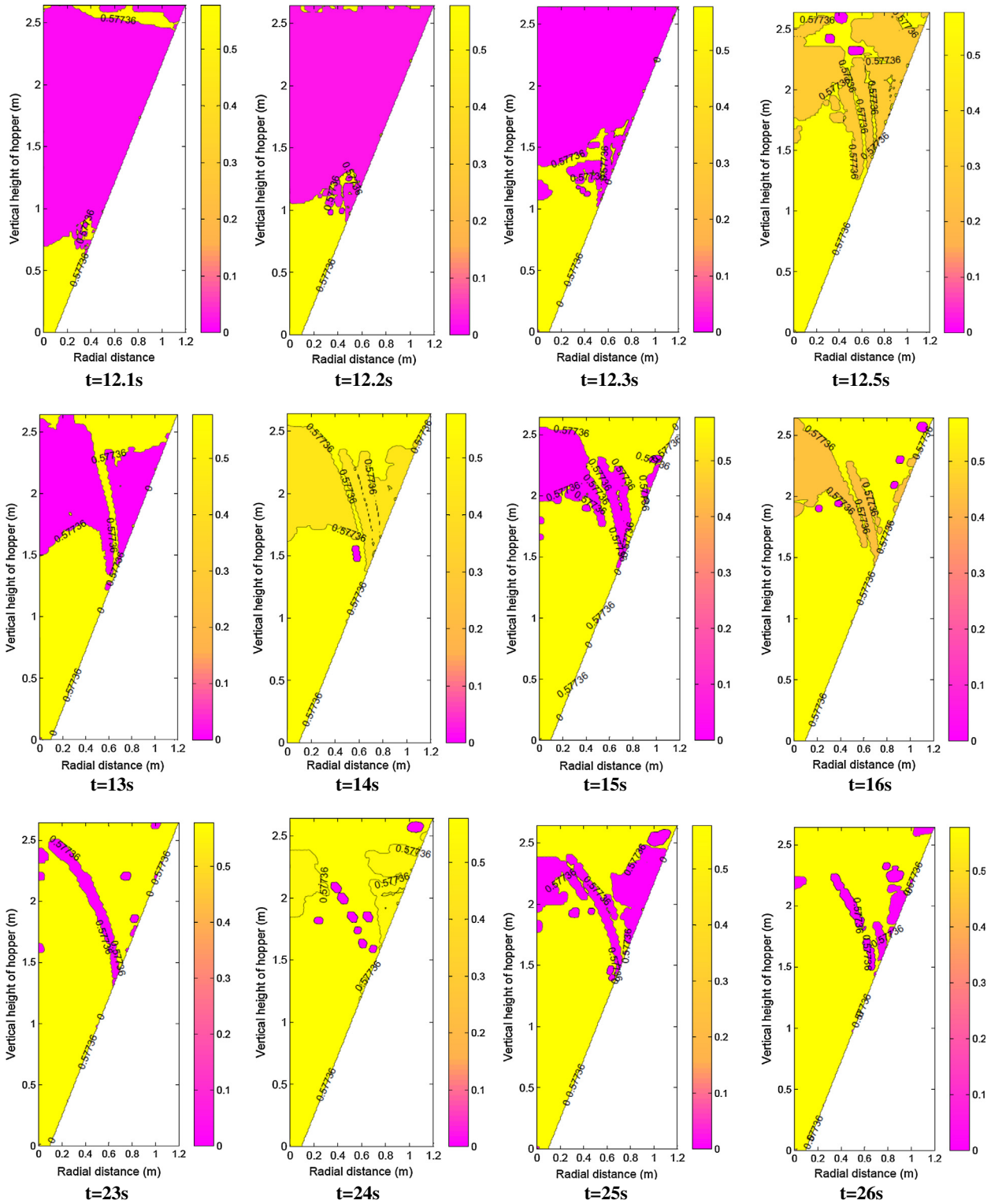

Fig. 17. Contours of stress ratio (τ/p) at various discharge time points under free flow.

clearly seen that the peaks of normal pressure and shear stress propagate very quickly from a lower height to a higher level. This occurs as the hopper outlet is opened and the solid begins to flow, the stress level at the bottom decreases towards zero. The normal pressures p_{wn} and shear stress p_{ws} on the wall tend to increase higher up in order to fulfil the equilibrium of forces. This change in wall pressure from filling state to discharge state is also associated with a switch of principal stress directions to an "arched" field as shown in Fig. 6. Fig. 9 shows the time series of the normal wall pressure at several locations on the hopper walls. It is clearly seen that the peak pressure occurs just after discharge starts, which can be associated with the peak progressing upwards rapidly as shown

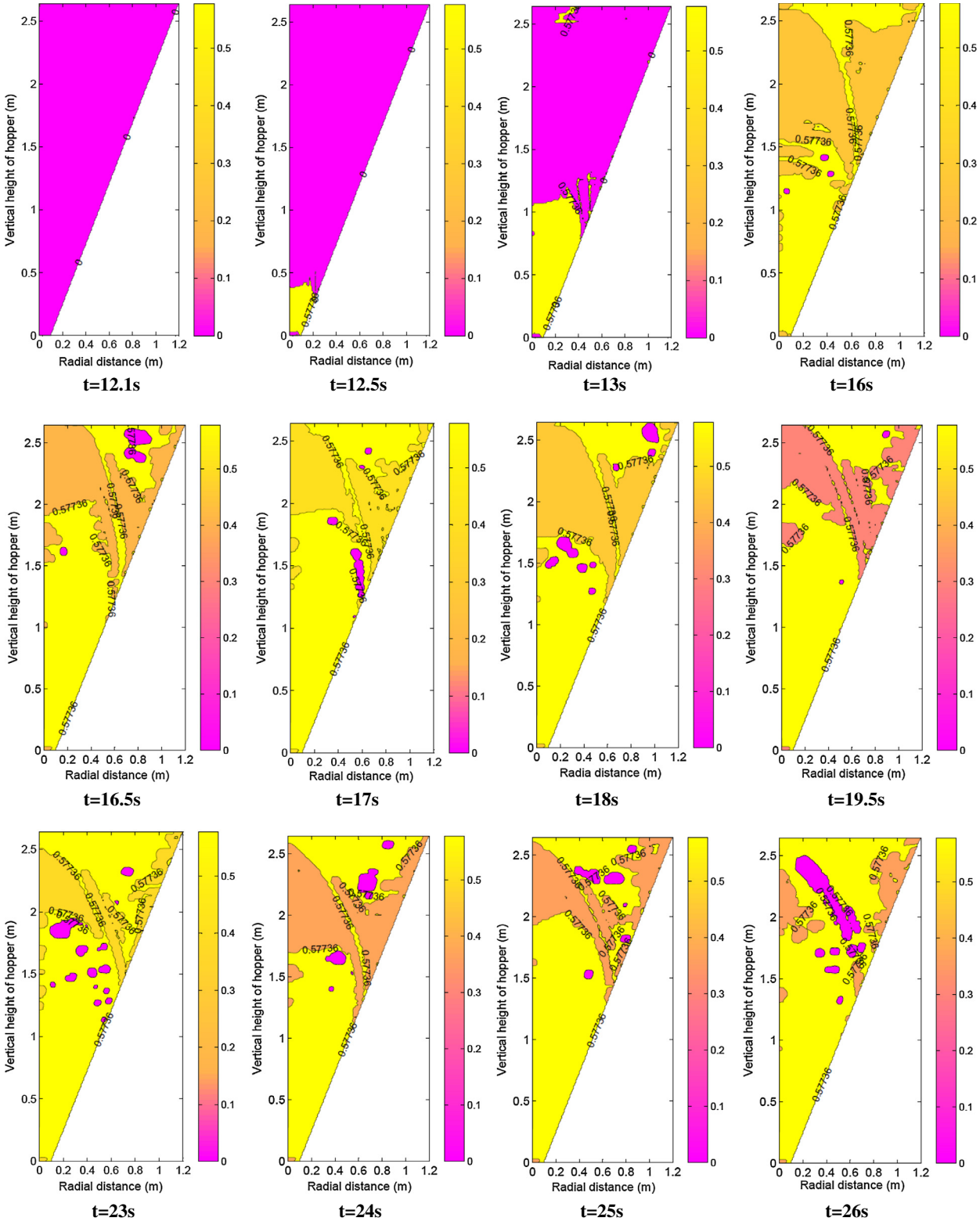

Fig. 18. Contours of stress ratio (τ/p) at various discharge time points under controlled flow ($u = 0.5u_0$).

in Fig. 8. Such an observation has been reported in a real hopper experiment [31].

5.2. Wall pressure and pressure fluctuation

It is generally known that a steady state flow can be reached during silo discharge [31], the instantaneous pressure is expected to always exhibit an oscillatory characteristic with amplitudes of greater than mean pressure and with certain frequencies [31–33]. Fig. 10(a) shows the time series of normal wall pressure at three different positions (point *a*, *e* and *f*) at the hopper walls during the discharge process. These pressures indeed exhibit fluctuating patterns which are similar to the fluctuations of discharge pressure reported in the experiments by Ostendorf et al. [31], as shown in Fig. 10(b). Note that in the experiment the discharge was under a controlled flow at a relatively slow speed, whereas in the numerical simulation herein the outflow has been assumed under gravity. Nevertheless, the pressure fluctuation phenomenon shows similar characteristics.

In order to understand the cause of the fluctuations, the frequency contents in the pressure series are analysed using a power spectral density estimation. The power spectral density estimation of the whole time series of discharge pressure at the representative point *e* in the present FE simulation is shown in Fig. 11. Two dominant frequencies can be identified from these spectra, one at less than 1 Hz and the other at about 5 Hz. Detailed discussions on the causes for these two frequency events will be given in Section 6.

To further examine the dynamic effect during hopper discharge, the computed wall shear stress is also investigated. The shear stress at the typical point *e* on the hopper wall is compared with the normal pressure, as shown in Fig. 12. It is noted that the shear stress appears to have a similar fluctuating pattern as the normal pressure.

The mobilised friction ratio of the shear stress to the normal pressure at a point on the wall can be evaluated as:

$$\mu_0 = \frac{p_{ws}}{p_{wn}} \tag{10}$$

where p_{ws} is the wall shear stress, and p_{wn} is the wall normal pressure. The coefficient of wall friction μ_w is set as 0.267 ($\phi_w = 15°$) in the simulation. Wall friction remains fully mobilised throughout the discharge simulation.

5.3. Internal stress within the granular solid

In addition to the wall pressure, the internal stress within the granular solid has also been analysed for the present axisymmetric FE model. Vertical and radial stresses are investigated here. The locations of sections (three generator and four horizontal sections) and points of interrogation are shown in Fig. 13. Fig. 14 shows the time series of the radial stress at various points within the solid during discharge. The radial stress at point *e*1, which is located very close to the wall, exhibits oscillatory characteristics and has similar pattern to the wall normal pressure at point *e*. That is, the fluctuation with the large amplitude has a frequency of less than 1 Hz and the small amplitude fluctuation has a frequency of ~5 Hz. Along the same horizontal line, the stresses at points *e*1, *e*2 and *e*3 away from the wall are characterised by fluctuations at the same frequencies, as shown in Fig. 14(a). In the generator direction (section 1-1), the radial stress apparently exhibits oscillatory characteristics all through the hopper. The key difference is that the magnitudes of the stress fluctuation increases from the hopper outlet upwards, as shown in Fig. 14(b). This is because as the distance from the outlet increases, it gradually approaches an intermittent arching shear zone, thus, the fluctuation increases accordingly. A detailed discussion about the intermittent arching shear zone is presented later in Section 6 of this paper. The distributions of radial stress in the three sections (1-1, 2-2 and 3-3) are shown in Fig. 15. The stress oscillations become stronger in the vicinity of the central axis of the hopper. In general, the magnitudes of radial stress decrease over time as the granular solid is discharged.

The distributions of the vertical stress along two typical sections (*e*-*e* and *b*-*b*) are shown in Fig. 16. These stresses are plotted as instantaneous values at a certain time point. It can be seen that non-uniform stresses along these horizontal sections evolve during discharge with the vertical stress decreasing progressively as the granular solid is withdrawn.

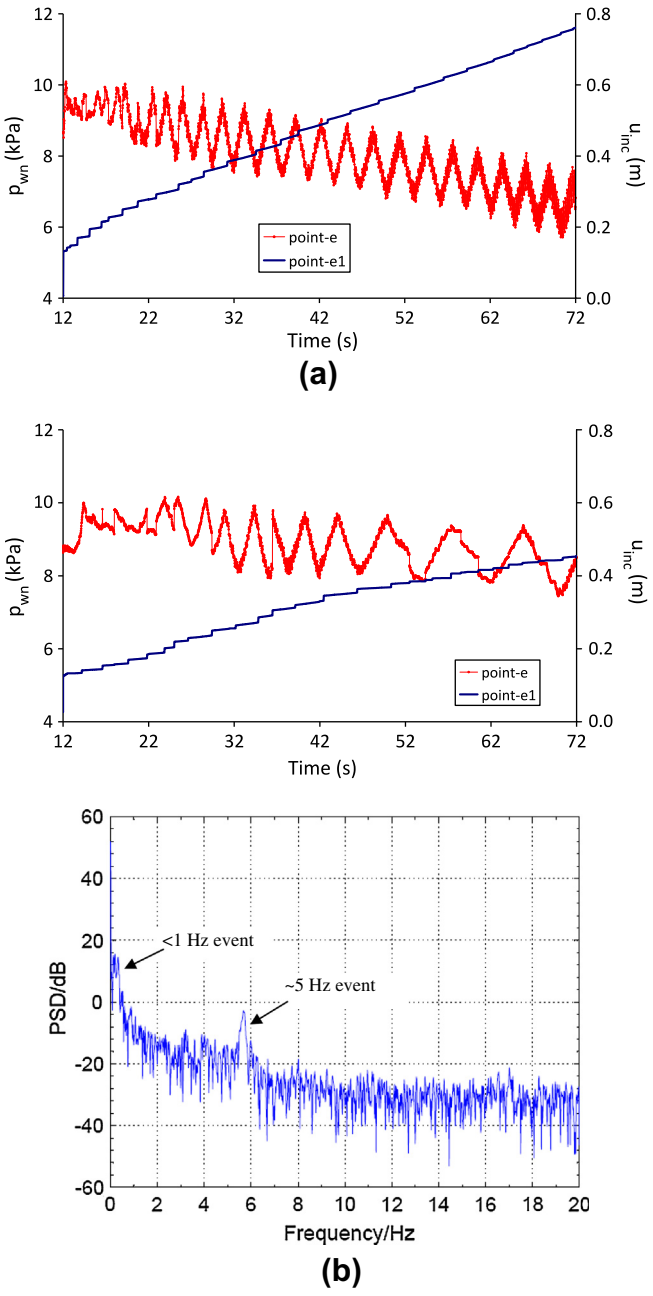

Fig. 19. Wall normal pressure (p_{wn}) at point *e* and slip displacement (u_{inc}) at point *e*1 at the hopper wall: (a) free flow; (b) controlled flow ($u = 0.5u_0$) and power spectral density estimation of wall pressure at point *e* for the whole process of discharge (t = 12–72 s).

6. Discussion on dynamic pressure

The dynamic events in wall pressure have been reported in many silo experiments, and explanations have generally been directed towards the pressure wave or stress discontinuity [6,7,31,34]. The present numerical results are studied further here to provide more insight into the nature and causes of the dynamic events observed in real silo and hoppers.

For the wall pressure fluctuation at much larger amplitudes of greater than 20% of mean pressure and with frequencies of less than 1 Hz, it may be examined from the view point of the evolution of shear zone which is associated with intermittent slip wall motion during discharge. The shear failure zone can be identified by high shear stress value which can be evaluated as the ratio μ of deviatoric stress τ to hydrostatic stress p within the granular solid as follows

$$\mu = \tau/p \tag{11}$$

The input angle of internal friction of 30° for the material in the present simulation gives a limiting stress ratio μ of 0.5773 when the Drucker–Prager failure criterion is used [14].

The propagation of the shear failure zones during discharge is depicted in Fig. 17. The shear failure zone is characterised by the light colour in the contour plot, while the darker colours correspond to non-failure (elastic) zones. A fixed coordinate system is used when extracting these contours, where the location of each material node corresponds to its un-deformed coordinate. This is purely for the convenience of plotting the stress contours, and should not affect the inspection when the overall drop of solid level is still not so large. Fig. 17 shows that at the initiation of discharge, the failure zone propagates upwards from the outlet until a large proportion of the solid is at plastic failure. At some point, an intermittent non-failure arching zone forms in the upper half of the hopper. It should be noted that the size of the arching zone in the present simulation may depend, to a certain extent, on the mesh size since the constitutive model employed does not involve a characteristic length relating to the micro-structure of granular solid. The formation and re-formation of this non-failure shear zone is linked with the predicted fluctuations in wall pressure. A similar effect has been discussed in the silo experiment by Blair-Fish and Bransby [34]. The corresponding states for the simulation with a slower controlled flow ($u = 0.5u_0$) are shown in Fig. 18. Comparing the two, it is found that the slower discharge case presents longer recurrence periods of the arching shear zone than the faster free flow case.

Associated with these intermittent arching shear zones in the solid, the displacement of the solid adjacent to the wall exhibits a continuous gradual slip motion interspersed with the intermittent macro-slips as shown in Fig. 19. Careful interrogation of the results shows that each of these macro-slips corresponds to a reduced shear stress ratio in the arching zone identified and the occurrence of a fluctuation in wall pressure. The frequency of these

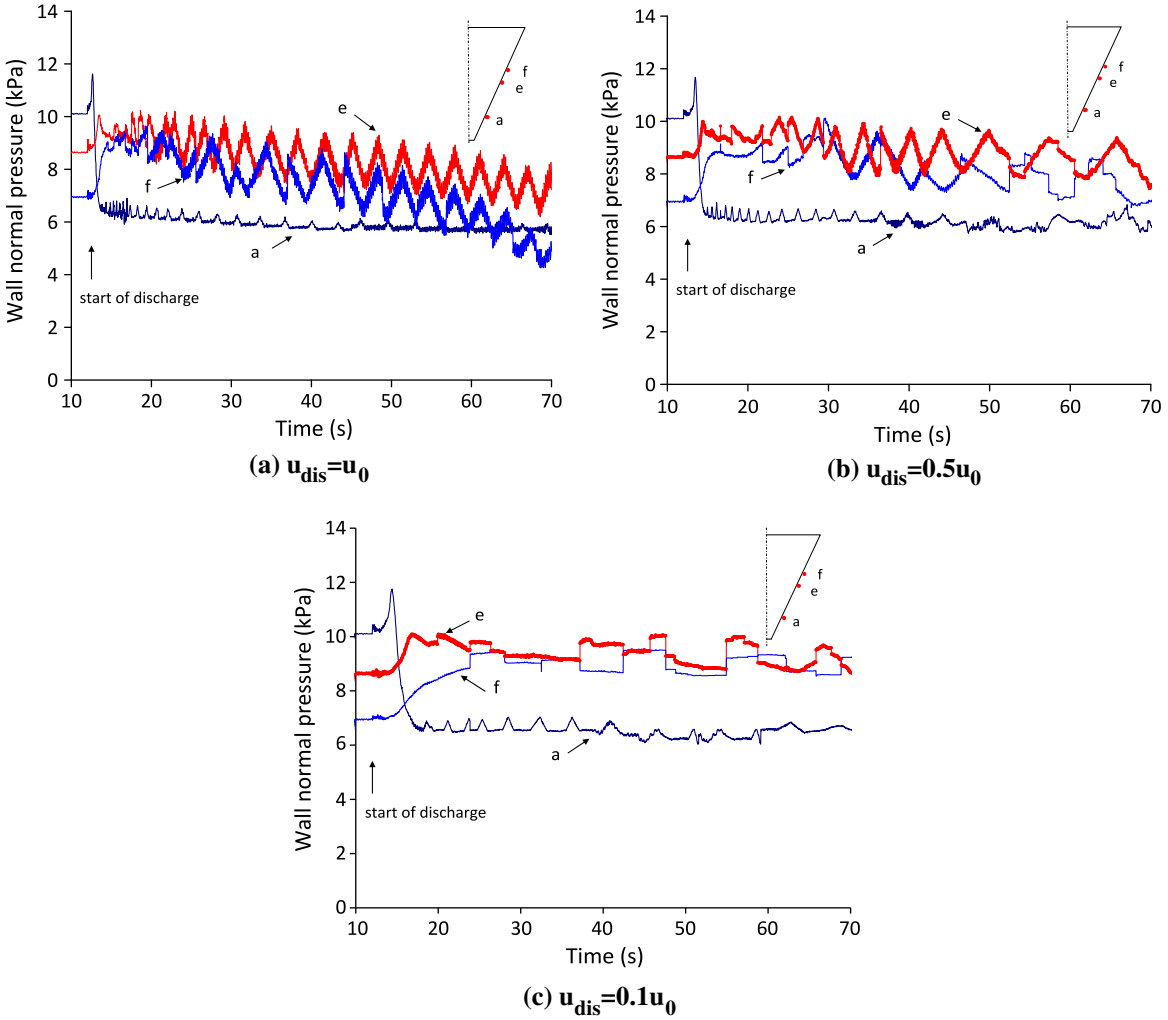

Fig. 20. Normal wall pressure at different wall points under three different discharge velocity regimes.

intermittent macro-slips and the intermittent shear zone are all less than 1 Hz, which is consistent with the larger wall pressure fluctuations and thus provides a reasonable explanation. It is worth noting that the general phenomenon of slip-stick motion or intermittent macro-slips have been observed in silo experiments [6,35].

With regard to the minor pressure fluctuation with a frequency of about 5 Hz, it may be explained by the longitudinal wave propagation within the granular solid stored in the hopper. The frequency of any longitudinal wave travelling within the granular solid in the hopper can be estimated from the wave equation for an elastic bar of hopper height with free ends [36]:

$$f_n = \sqrt{\frac{E(1-\upsilon)}{\rho_b(1+\upsilon)(1-2\upsilon)}}/2h_f = \sqrt{\frac{550000(1-0.3)}{1000(1+0.3)(1-2\times 0.3)}}/2\times 2.64 \cong 5.2Hz \quad (12)$$

where E denotes the Young's modulus, υ is the Poisson's ratio, ρ_b is the bulk density of the granular solid and h_f is the height of the fill in the hopper. This confirms that the 5 Hz fluctuation at small amplitudes in the FE calculated pressure is caused by the longitudinal wave propagation.

7. Influence of other key parameters

Two key parameters, namely the discharge velocity and the wall roughness, are expected to influence the dynamic events in real silos and hoppers [35,37,38]. The influences of these parameters during hopper discharge are further investigated here using the numerical model.

7.1. Effect of discharge velocity

The time series for the computed normal wall pressure at three different positions on the hopper walls for different controlled discharge velocity profiles ($u_{dis} = u_0$, $0.5u_0$, $0.1u_0$) are shown in Fig. 20. As the discharge velocity decreases from high flow rate as shown in Fig. 20(a) to lower flow rate in (b) and (c), the occurrence and magnitude of pressure fluctuation diminish. In particular in the region surrounding point *e* and *f*, the low frequency (high amplitude) fluctuations in the pressure computed for high flow rate can be seen to reduce in amplitude and to a lesser extent the frequency as velocity decreases to $u_{dis} = 0.5u_0$. When the velocity is reduced even further to the $u_{dis} = 0.1u_0$ case, the pressure oscillation has largely disappeared and is replaced by the intermittent step-change in pressure. This decreasing dynamic effect in wall pressure concurs with reported observation that silo dynamic effects such as silo quaking, shock loads and silo honking diminish in magnitude and frequency of occurrence at lower discharge rates [6,35].

7.2. Effect of wall roughness

The FE simulation with smooth hopper walls where the coefficient of wall friction μ_w is set to a very small value of 0.01 has also been performed and it is used to compare with the reference case with hopper walls where the coefficient of wall friction μ_w is set to 0.267 (see Fig. 21). In Fig. 21(a), contours are shown of the tracers used to track the motion of solid particles at various discharge time points in the FE simulation. These contours indicate that mass flow is obtained during discharge for both cases. With negligible wall friction, the material moves at a faster discharge rate out of the hopper and with a more uniform velocity and stress profile across horizontal sections. Comparison of the pressure–time plots, as shown in Fig. 21(b), indicates that large amplitude–low frequency pressure oscillations are only present for the walls simulation with

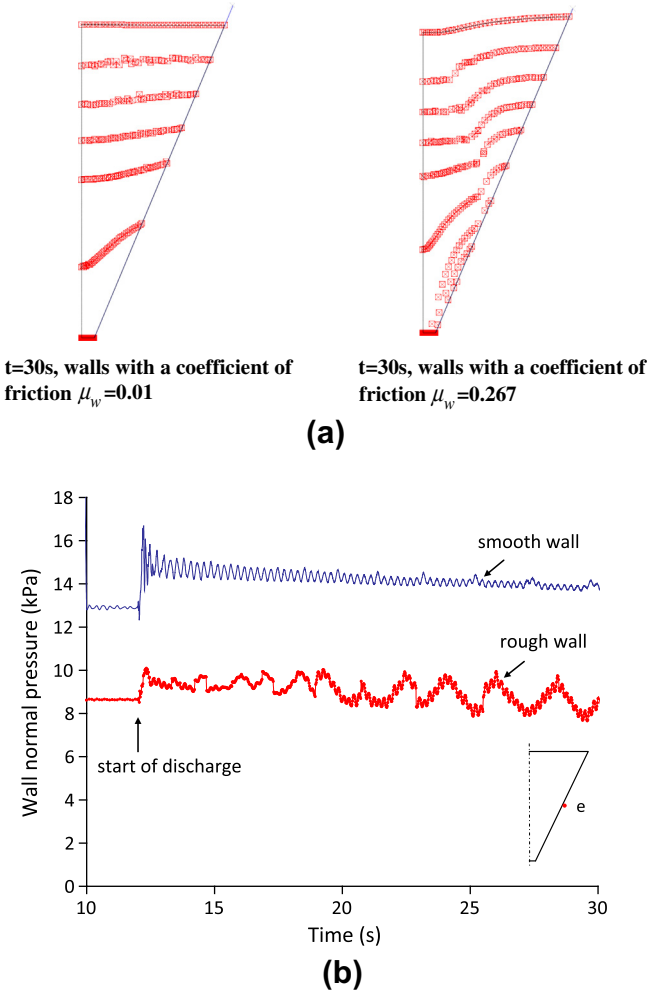

Fig. 21. Comparison of FE results between walls with a coefficient of friction $\mu_w = 0.01$ and $\mu_w = 0.267$: (a) contours of flow pattern at $t = 30$ s; (b) time series of normal wall pressure at point *e*.

a coefficient of friction $\mu_w = 0.267$ whilst the fluctuations for the smooth walls case are caused only by the longitudinal wave propagation in the granular solid which are considerably smaller in amplitudes. It is evident that the presence of wall roughness is an essential element for inducing the intermittent macro-slips and the intermittent shear failure zones within the solid which lead to the significant wall pressure fluctuations. The important role of the wall roughness has also been observed in some experimental studies of silo quaking [38,39], so there is some limited evidence that dynamic pressure observed during silo discharge is significantly influenced by the presence of wall friction.

8. Conclusions

The FE model using the ALE formulation has been shown to be an effective technique for the simulation of silo discharge process which involves large plastic deformations. By defining an adaptive mesh for the granular solid and suitable boundary conditions for the mesh region, it is possible to model in principle almost an entire process of the discharge in a satisfactory manner.

The discharge pressure distribution and the mass flow rate predicted using the present FE model are in good agreement with the theoretical solutions. The transient dynamic phenomena induced by the silo discharge, in particular the dynamic fluctuations of pressure, are found to exhibit two primary frequencies (about

5 Hz and less than 1 Hz). Detailed analysis of the results has shown that the higher frequency event is attributable to the stress wave propagation within the granular solid, while the event with low frequency (less than 1 Hz) and much larger amplitude is associated with the intermittent arching shear zones within the flowing material and the associated intermittent macro-slips between the granular solid and the walls. This study has shown that instead of a slip-stick wall motion, a steep mass flow hopper can exhibit a continuous gradual slip motion interspersed with the intermittent macro-slips. These macro-slips have been shown to be associated with significant wall pressure fluctuations that could be a source of vibration problems observed in some silos.

Further parametric study with the FE model has been performed to investigate the effect of discharge velocity and wall roughness. Both the frequency and the amplitude of the large fluctuations in wall pressure are reduced as the discharge velocity decreases. The presence of wall roughness appears to be an essential element for inducing intermittent macro-slips and arching shear zone within the solid, giving rise to the dominant wall pressure fluctuation with larger amplitude and smaller frequency.

References

[1] Janseen HA. Versuche uber getreidedruck in silozellen. Z Vereines Deuischer Ingenieur 1895;39(35):1045–9.
[2] Rotter JM. Guide for the economic design of circular metal silos. London: Spon Press; 2001.
[3] Hartlen J, Nielsen J, Ljunggren L, Martensson G, Wigram S. The wall pressure in large grain silos. Swedish Council for Building Research, Document D2, Stockholm; 1984.
[4] Ooi JY, Rotter JM. Measured pressures in full scale silos: a new understanding. In: Proc bulk 2000: bulk mat handling-towards the year 2000. Institute of Mechanical Engineers, London; 1991. p. 195–200.
[5] Brown CJ, Jarrett ND, Moore DB. Pressures in a square planform silo during discharge. Proc Inst Mech Eng, Part E: J Process Mech Eng 1996;210(E2):101–8.
[6] Roberts AW. Shock loads in silos, the silo quaking problem. Bulk Solids Handl 1996;16(1):59–73.
[7] Ramirez A, Nielsen J, Ayuga F. On the use of plate-type normal pressure cells in silos. Part 2: Validation for pressure measurements. Comput Electron Agric 2010;71:64–70.
[8] Ooi JY, Rotter JM. Wall pressure in squat steel silos from simple finite element analysis. Comput Struct 1990;37(4):361–74.
[9] Goodey RJ, Brown CJ, Rotter JM. Predicted patterns of filling pressure in thin-walled square silos. Eng Struct 2006;28:109–19.
[10] Chen JF, Yu SK, Ooi JY, Rotter JM. Finite-element modelling of filling pressure in a full-scale silo. J Eng Mech 2010;127(10):1058–66.
[11] Rombach G, Eibl J. A dynamic finite element model for silo pressure and solids flow. In: Brown CJ, Nielsen J, editors. Silos, fundamentals of theory behaviour and design. E&FN SPON; 1998. p. 481–94.
[12] Martinez MA, Alfaro I, Doblare M. Simulation of axisymmetric discharging in metallic silos: analysis of the induced pressure distribution and comparison with different standards. Eng Struct 2002;24:1561–74.
[13] Vidal P, Guaita M, Ayuga F. Analysis of dynamic discharge pressures in cylindrical slender silos with a flat bottom or with a hopper: comparison with Eurocode 1. Biosyst Eng 2005;91(3):335–48.
[14] SIMULIA. Abaqus analysis: User's manual. Dassault Systemès; 2008.
[15] Tejchman J, Gudehus G. Silo-music and silo-quake experiments and a numerical Cosserat approach. Powder Technol 1993;76:201–12.
[16] Zienkiewicz OC, Taylor RL, Zhu JZ. The finite element method: its basis and fundamentals. Elsevier; 2005.
[17] Walker DM. An approximate theory for pressures and arching in hoppers. Chem Eng Sci 1966;21:975–97.
[18] Nedderman RM. Statics and kinematics of granular materials. Cambridge: Cambridge University Press; 1992.
[19] EN 1991-4. Eurocode 1: actions on structures. Silos and tanks. Brussel: CEN; 2006.
[20] Beverloo WA, Leniger HA, Van de Velde J. The flow of granular solids through orifices. Chem Eng Sci 1961;15:260.
[21] Rose HF, Tanaka T. Rate of discharge of granular materials from bins and hoppers. Engineer 1956;208:465.
[22] Wojcik M, Tejchman J. Modeling of shear localization during confined granular flow in silos within non-local hypoplasticity. Powder Technol 2009;192:298–310.
[23] Donéa J, Huerta A. Finite element methods for flow problems. Wiley Press; 2003.
[24] Drucker DC, Prager W. Soil mechanics and plastic analysis on limit design. Quart Appl Math 1952;10(2):157–65.
[25] Ayuga F, Guaita M, Aguado P. Static and dynamic silo loads using finite element models. J Agric Eng Res 2001;78(3):299–308.
[26] Yang Y, Ooi JY, Rotter JM, Wang Y. Numerical analysis of silo behavior using non-coaxial models. Chem Eng Sci 2011;66:1715–27.
[27] Wang Y, Wensrich CM, Ooi JY. Rarefaction wave propagation in tapered granular columns. Chem Eng Sci 2012;71:32–8.
[28] Ai J, Chen JF, Rotter JM, Ooi JY. Numerical and experimental studies of the base pressures beneath stockpiles. Granular Matter 2011;13:133–41.
[29] Ooi JY, Rotter JM. Elastic prediction of pressures in conical silo hoppers. Eng Struct 1991;13(1):2–12.
[30] Karlsson T, Klisinski M, Runesson K. Finite element simulation of granular material flow in plane silos with complicated geometry. Powder Technol 1998;99:29–39.
[31] Ostendorf M, Schwedes J, Bohrnsen JU, Antes H. Dynamic measurement and simulation of bulk solids during silo discharge. Task Quart 2003;7(4):611–21.
[32] Nielsen J. Pressures from flowing granular solids in silos. Philos Trans R Soc Lond A 1998;356:2667–84.
[33] Bohrnsen JU, Antes H, Ostendorf M. Silo discharge: measurement and simulation of dynamic behavior in bulk solids. Chem Eng Technol 2004;7(1):71–6.
[34] Blair-Fish PM, Bransby PL. Flow patterns and wall stresses in a mass-flow bunker. J Eng Ind, ASME 1973;B95(1):17–26.
[35] Wensrich C. Experimental behaviour of quaking in tall silos. Powder Technol 2002;127:87–94.
[36] Prakash S. Soil dynamics. New York: McGraw-Hill; 1981.
[37] Muite BK, Quinn SF, Sundaresan S, Rao KK. Silo music and silo quake: granular flow-induced vibration. Powder Technol 2004;145:190–202.
[38] Tejchman J. Technical concept to prevent the silo honking. Powder Technol 1999;106:7–22.
[39] Schulze D. Time- and velocity-dependent properties of powders effecting slip-stick oscillations. Chem Eng Technol 2003;26(10):1047–51.